J. Fluid Mech. (1985), *vol.* 152, *pp.* 173–190
Printed in Great Britain

An algorithm for the use of the Lagrangian specification in Newtonian fluid mechanics and applications to free-surface flow

By POUL BACH AND OLE HASSAGER
Instituttet for Kemiteknik, Danmarks Tekniske Højskole, Lyngby, Denmark

(Received 8 May 1984)

An algorithm is constructed for the use of the Lagrangian kinematic specification in Newtonian fluid mechanics. The algorithm is implemented with a finite-element method, and it is demonstrated that the method accurately describes free-surface flow, including the effects of surface tension, with the use of just bilinear isoparametric elements. Moving contact lines are modelled with a small amount of slip near the contact lines. The contact angle boundary condition is included in the form of a net interfacial force specified at the contact line. Simulations of measurements in a parallel-plate geometry show that the measured apparent contact angle is not the true angle, and that the true angle is always very close to the equilibrium value.

1. Introduction

The purpose of this paper is to construct an algorithm for the use of the Lagrangian specification of fluid flow and to illustrate its application in a series of flow situations with free surfaces and dynamic wetting lines. The Lagrangian kinematic specification has been used relatively little compared to the Eulerian specification. One reason for this may be that the conservation equations in Lagrangian form present an initial-value problem. Thus one is forced to include time as an independent variable even in situations where the aim is to describe a flow that is steady in the Eulerian specification, and in situations when an analytical solution is desired that is certainly inconvenient. In other situations, however, it may not be possible to obtain analytical solutions in closed form, and then the solution procedure will involve an iterative process even when the Eulerian specification is used. In such situations we feel that the time variable present in the Lagrangian formulation is now a convenient parameter to use in the iteration process. In §2 we demonstrate how an iterative process may be used to obtain a simple Lagrangian statement of the conservation equations for an incompressible Newtonian fluid, and in §3 this is converted to an algorithm. The method is an extension of that introduced by Bach & Hassager (1984) and used also by Bach & Villadsen (1984). An early application of the Lagrangian specification was that of Hirt, Cook & Butler (1970).

In §4 we apply the formulation to the flow near a meniscus of a fluid contained between two parallel planes sliding relative to each other with fixed separation. In §5 we consider subsequently the flow near the moving meniscus of a fluid advancing in the space between two fixed parallel planes. Both of these flow situations involve two interesting aspects of free-surface flow. These are: first, the flow in the immediate neighbourhood of a moving contact line where fluid contacts a solid wall; and, secondly, the question of locating the free boundary, which is a somewhat inconvenient additional unknown variable when an Eulerian specification is used.

The flow near a moving line of contact between a solid surface and a free surface

was considered by Moffatt (1964). In this development the free surface was assumed to be flat and a solution was obtained which was valid in the neighbourhood of the contact line, but not at the contact line where a non-integrable stress singularity is predicted. In order to remedy this situation, Huh & Mason (1977) and Hocking (1981) introduced the physical model of minute slip at the contact line. This model was also used by Lowndes (1980) in a finite-element simulation of a moving meniscus and we will adopt it here. The correct treatment of a dynamic contact line is still not completely resolved. For example the molecular interpretation of slip is not understood, and the notion may be questioned. Also, from a practical point of view, the above model is useful primarily at low capillary numbers where surface-tension effects are important. At intermediate capillary numbers we will demonstrate that surface tension is important only in a small 'boundary layer' near the contact line. At high capillary numbers a model in which fluid is 'rolled' onto or off a solid boundary may be needed. More information on dynamic wetting lines is found in Hocking (1981) and Kistler & Scriven (1983).

The question of locating a free surface presents a difficulty when an Eulerian specification is used and the aim is to obtain a steady-state solution. As outlined previously, and reiterated recently by Tanner (1983) three boundary conditions are to be satisfied simultaneously at the free surface: (i) zero normal velocity; (ii) zero (or prescribed) shear stress; (iii) normal stress balanced by surface tension and external pressure.

The most commonly used technique that deals with this situation is an iterative procedure in which one condition is ignored, the flow problem is then solved with the remaining two conditions for an assumed shape, the ignored condition is then used to change the shape and the flow problem is again solved with the remaining two conditions for the new shape, and so on. As outlined by Tanner (1983) the condition iteratively ignored should be either (i) or (iii) depending on the ratio of surface tension to viscous forces. Certainly this procedure is not very satisfactory. Another technique is that of Ruschak (1980), who included the location of the surface as a dependent variable. All three boundary conditions may then be included in the solution procedure at the same time. In the Lagrangian formulation, however, the location of the free surface is already included among the dependent variables and presents no extra complication. Only conditions (ii) and (iii) are applied at the surface. Condition (i) will in general not be satisfied, but it holds if a steady state is ultimately reached.

Finite-element codes are somewhat more lengthy to implement than finite-difference codes. For this reason a finite-element code should be formulated sufficiently generally such that a large number of physical problems can be described. In §6 we illustrate briefly the generality of the present implementation by considering a slide-coating operation where a thin layer of liquid is deposited on a moving surface.

2. Lagrangian finite-element method

To illustrate the fluid-mechanical content of the formulation, we begin with the equations of conservation of linear momentum and mass for incompressible Newtonian fluids in the conventional Eulerian form:

$$\rho\left(\frac{\partial}{\partial t}+v_m\frac{\partial}{\partial x_m}\right)v_i=-\frac{\partial}{\partial x_i}p+\mu\frac{\partial}{\partial x_m}\left(\frac{\partial v_i}{\partial x_m}+\frac{\partial v_m}{\partial x_i}\right)+\rho g_i \quad (i=1,2,3), \tag{2.1}$$

$$0=\frac{\partial}{\partial x_m}v_m. \tag{2.2}$$

Here the $v_i = v_i(x,t)$ are the components of the velocity field in a Cartesian coordinate system x_i $(i = 1,2,3)$ and x is used as shorthand for (x_1, x_2, x_3). In (2.1) and (2.2) ρ is the density, $p = p(x,t)$ the pressure, μ the viscosity, g_i with $i = 1,2,3$ the components of the gravitational acceleration and t is time. We use the convention that the total stress tensor π_{ij} is given by

$$\pi_{ij} = p\delta_{ij} - \mu\left(\frac{\partial v_i}{\partial x_j} + \frac{\partial v_j}{\partial x_i}\right). \tag{2.3}$$

Furthermore, given a surface element $\mathrm{d}S$ with orientation defined by the unit normal, n_i, then the force exerted by the fluid on the negative side of $\mathrm{d}S$ on the fluid on the positive side of $\mathrm{d}S$ has components i given by $n_j \pi_{ji}$ (Bird, Armstrong & Hassager (1977)). Obviously, some of the terms in (2.1) may be eliminated by the use of (2.2) but we retain the terms for later use.

To arrive at a Lagrangian formulation, we must formulate the conservation equations in such a way that the coordinates x_i appear as dependent variables and the independent variables are instead fluid particle labels. The particle labels are conveniently defined by the particle coordinates x_i^0 at reference time t_0. The coordinates, when viewed as functions of particles and time, are then expressed as the displacement functions $x_i = x_i(x^0, t_0, t)$ where $x^0 = (x_1^0, x_2^0, x_3^0)$. The other dependent variables are the Lagrangian velocity field $u_i = u_i(x^0, t_0, t)$ and the Lagrangian pressure field $p = p(x^0, t_0, t)$. The Lagrangian velocity field is related to the coordinates by the definition:

$$\frac{\partial}{\partial t} x_i(x^0, t_0, t) = u_i(x^0, t_0, t). \tag{2.4}$$

To arrive at the conservation statements we substitute $u_i(x^0, t_0, t)$ and $p(x^0, t_0, t)$ for $v_i(x,t)$ and $p(x,t)$ in (2.1) and (2.2). In so doing we use the chain rule of partial differentiation only on the left-hand side of (2.1):

$$\rho \frac{\partial}{\partial t} u_i(x^0, t_0, t) = -\frac{\partial}{\partial x_i} p(x_0, t^0, t) + \mu \frac{\partial}{\partial x_m}\left(\frac{\partial u_i}{\partial x_m} + \frac{\partial u_m}{\partial x_i}\right) + \rho g_i, \tag{2.5}$$

$$0 = \frac{\partial}{\partial x_m} u_m(x^0, t_0, t). \tag{2.6}$$

In this form we recognize the simplification of the inertial terms on the left-hand side of (2.5), characteristic of a Lagrangian formulation. The price paid for this simplification is apparent on the right-hand side of (2.5) and (2.6) where the differentiations are with respect to the coordinates x_i that we wish to determine. The most natural procedure might then seem to be to use the chain rule also on the right-hand side of these equations. This process brings in the relative deformation gradient, $\partial x_i^0 / \partial x_j$, which is in turn expressed through its inverse $\partial x_j / \partial x_i^0$. In this work, however, we use a different procedure in which we arrive at the unknown coordinates, velocities and pressures through an iterative process. In each iteration where $\nu = 0, 1, 2, \ldots$, we solve the following equations for the velocities $u_i^{\nu+1}$ and pressures $p^{\nu+1}$:

$$\rho \frac{\partial}{\partial t} u_i^{\nu+1}(x^0, t_0, t) = -\frac{\partial}{\partial x_i^\nu} p^{\nu+1}(x^0, t_0, t) + \mu \frac{\partial}{\partial x_m^\nu}\left(\frac{\partial u_i^{\nu+1}}{\partial x_m^\nu} + \frac{\partial u_m^{\nu+1}}{\partial x_i^\nu}\right) + \rho g_i; \tag{2.7}$$

$$0 = \frac{\partial}{\partial x_m^\nu} u_m^{\nu+1}. \tag{2.8}$$

Here the x_i^ν are the coordinates obtained in the previous iteration. The coordinates are then updated through the use of (2.4):

$$x_i^{\nu+1}(x^0, t_0, t) = x_i^0 + \int_{t'=t_0}^{t} u_i^{\nu+1}(x^0, t_0, t')\,\mathrm{d}t'. \tag{2.9}$$

The coordinates $x_i^{\nu+1}$ from (2.9) are then used in (2.7) and (2.8) to determine $u_i^{\nu+2}$ and $p^{\nu+2}$ and so on. The process is initiated with the reference configuration x_i^0 for $\nu = 0$ in (2.7) and (2.8). If the process converges so that $x_i^\nu \sim x_i^{\nu+1}$ for sufficiently large ν, then (2.7), (2.8) and (2.9) become equivalent to (2.4), (2.5) and (2.6), with the Lagrangian variables given by:

$$x_i = \lim_{\nu\to\infty} x_i^\nu; \tag{2.10}$$

$$u_i = \lim_{\nu\to\infty} u_i^\nu; \tag{2.11}$$

$$p = \lim_{\nu\to\infty} p^\nu. \tag{2.12}$$

Equations (2.7) and (2.8) are similar in form to (2.1) and (2.2) merely with the nonlinear term absent in (2.1), and it may seem surprising at first that the above scheme provides a truly transient solution. Keep in mind, however, that the x_i in (2.1) and (2.2) are fixed, whereas the x_i in (2.7) and (2.8) are changed in the iterations. The procedure described so far does not involve any discretization assumptions. We turn now to the question of how the procedure may be implemented in a numerical simulation of flow. In the Lagrangian formulation we discretize time and fluid material.

The discretization of time is performed by using the following two approximations for the time derivative appearing in (2.7) and the integral in (2.9):

$$\frac{\partial}{\partial t} u_i^{\nu+1}(x^0, t_0, t) = \frac{u_i^{\nu+1}(x^0, t_0, t) - u_i^0(x^0, t_0, t_0)}{t - t_0}; \tag{2.13}$$

$$\int_{t'=t_0}^{t} u_i^{\nu+1}(x^0, t_0, t')\,\mathrm{d}t' = \tfrac{1}{2}(u_i^{\nu+1}(x^0, t_0, t) + u_i^0(x^0, t_0, t_0))\,(t - t_0). \tag{2.14}$$

Notice that these approximations require the current velocities to be reasonably close to the velocities in the reference configuration. The final time-marching scheme that appears then is the following: given an initial configuration and velocity field (x^0, u^0) at a time t_0, we update time by an amount Δt to $t = t_0 + \Delta t$, and iterate for the (x, u, p) at time t through (2.7) to (2.9) as explained above. Once the new configuration has been determined it is then chosen as the next reference configuration and time is again updated and so on. Provided that the individual time steps are chosen to be sufficiently small the iterative scheme in each time step is rapidly convergent.

The discretization of the fluid is performed by finite elements (see Cook 1974; or Chung 1978). This means that in each iteration in (2.7) and (2.8), the velocity field $u_i^{\nu+1}$ and pressure field $p^{\nu+1}$ are approximated by $\tilde{u}_i^{\nu+1}$ and $\tilde{p}^{\nu+1}$, where

$$\tilde{u}_i^{\nu+1} = \sum_{q=1}^{N} U_{iq}\,\phi^q(x^\nu); \tag{2.15}$$

$$\tilde{p}^{\nu+1} = \sum_{r=1}^{M} P_r\,\psi^r(x^\nu). \tag{2.16}$$

Here U_{iq} and P_r are values of velocities and pressures at key fluid particles called nodes, and the ϕ^q and ψ^r are global interpolation functions for velocities and pressure. When (2.15) and (2.16) are inserted in (2.7) and (2.8), and (2.13) is used, the results are residuals defined by

$$R_{ui}(x) = -\rho\frac{\partial}{\partial t}\tilde{u}_i^{\nu+1} - \frac{\partial}{\partial x_i^\nu}\tilde{p}^{\nu+1} + \mu\frac{\partial}{\partial x_m^\nu}\left(\frac{\partial\tilde{u}_i^{\nu+1}}{\partial x_m^\nu} + \frac{\partial\tilde{u}_m^{\nu+1}}{\partial x_i^\nu}\right) + \rho g_i; \tag{2.17}$$

$$R_p(x) = \frac{\partial}{\partial x_m^\nu}\tilde{u}_m^{\nu+1}. \tag{2.18}$$

We now define the following Galerkin form of the conservation equations:

$$\int_V R_{ui}(x)\,\phi^q\,\mathrm{d}V = 0, \quad q = 1,2,\ldots,N, \quad i = 1,2,3, \tag{2.19}$$

$$\int_V R_p(x)\,\psi^r\,\mathrm{d}V = 0, \quad r = 1,2,\ldots,M, \tag{2.20}$$

where R_{ui} and R_p are given by (2.17) and (2.18). Here V is the volume of the liquid in iteration ν and $\mathrm{d}V = \mathrm{d}x_1^\nu\,\mathrm{d}x_2^\nu\,\mathrm{d}x_3^\nu$. In order to reduce the degree of continuity required of the interpolation functions ϕ^q, we follow standard procedures (Chung 1978) whereby certain terms in (2.19) are integrated by the use of the Gauss theorem to yield in place of (2.17) and (2.19):

$$-\rho\frac{\partial}{\partial t}\int_V \tilde{u}_i^{\nu+1}\phi^q\,\mathrm{d}V + \int_V\left[\tilde{p}^{\nu+1}\frac{\partial\phi^q}{\partial x_i^\nu} - \mu\left(\frac{\partial\tilde{u}_i^{\nu+1}}{\partial x_m^\nu} + \frac{\partial\tilde{u}_m^{\nu+1}}{\partial x_i^\nu}\right)\frac{\partial\phi^q}{\partial x_m^\nu}\right]\mathrm{d}V$$
$$+\int_S f_i\phi^q\,\mathrm{d}S + \int_V g_i\phi^q\,\mathrm{d}V = 0, \quad q = 1,2,\ldots,N. \tag{2.21}$$

Here S is the surface of the fluid in iteration ν, and f_i is the external force (per unit area) exerted on the fluid in configuration ν, defined according to (2.3) by

$$f_i = -n_m\left[\tilde{p}^{\nu+1}\delta_{im} - \mu\left(\frac{\partial\tilde{u}_i^{\nu+1}}{\partial x_m^\nu} + \frac{\partial\tilde{u}_m^{\nu+1}}{\partial x_i^\nu}\right)\right], \tag{2.22}$$

where n_m is the mth component of the outwardly directed unit normal to the surface S.

We turn now to the introduction of boundary conditions. These conditions are divided into 'essential' and 'natural' conditions in the finite-element nomenclature.

An essential boundary condition is the specification of a velocity component. This condition is imposed by replacing the equation for the corresponding shape function ϕ^q in (2.21) by the statement $U_q = U_{qc}$, where U_{qc} is the desired value of the velocity of the node. The equation is subsequently eliminated from the global system of equations in such a way that the global system remains symmetric. Essential boundary conditions are satisfied exactly in the final solution.

A natural boundary condition is the specification of an external-force component on a surface. Such a condition is imposed by inserting the desired value of the force, f_i, in (2.21) instead of the expression in (2.22). Natural boundary conditions are not of necessity satisfied exactly in the final solution.

On each boundary node two conditions need to be specified, and these may be either two essential conditions, two natural conditions or one of each. Surfaces where two essential conditions are specified are denoted as 'no-slip surfaces'. Surfaces with one essential condition and one natural boundary condition (not in same direction) are

denoted 'slip surfaces', and surfaces with two natural boundary conditions are denoted 'free surfaces'. On a node that marks the intersection between a no-slip surface and a free surface, one essential condition and one natural condition are usually specified in a manner to be explained in the following.

We turn now to the implementation of natural boundary conditions on a free surface in the non-trivial situation when surface tension is considered important. In this situation f_i in (2.21) is given by

$$f_i = n_i(2H\sigma - P_{\text{ext}}), \tag{2.23}$$

where n_i is a component of the unit normal $\boldsymbol{n}$ to the surface, σ is the coefficient of surface tension and H is the mean curvature. Now, the mean curvature involves second derivatives of the surface location. The consequence of this is that a straightforward application of (2.23) in (2.21) would require elements with boundaries given by polynomials of at least second order and C^1 continuity where the elements join. In particular, the C^1 requirement is inconvenient, and following Ruschak (1980) we now demonstrate how this requirement may be reduced to C^0 for the special situation of plane flow.

We consider the two-dimensional situation in which the surface S is described by a curve in a plane. The arc length along this curve is denoted s. We start with the first Frenet formula (Sokolnikoff & Redheffer 1966) for the turning of the unit tangent vector $\boldsymbol{t}$ with increments in the arc length $\mathrm{d}s$:

$$(\mathrm{d}\boldsymbol{t}/\mathrm{d}s) = 2H\boldsymbol{n}. \tag{2.24}$$

When (2.24) is used in (2.23) we find that certain terms in (2.21) may be integrated by parts to yield

$$\int_{s_0}^{s_1} f_i \phi^q \,\mathrm{d}s = -\int_{s_0}^{s_1} n_i P_{\text{ext}} \phi^q \,\mathrm{d}s - \sigma \int_{s_0}^{s_1} t_i \frac{\mathrm{d}\phi^q}{\mathrm{d}s} \,\mathrm{d}s + \sigma[\phi^q t_i]_1 - \sigma[\phi^q t_i]_0. \tag{2.25}$$

Here the square brackets indicate that the quantities are to be evaluated at endpoints '1' and '0', respectively. Boundary conditions on free surfaces are therefore implemented as natural boundary conditions by substituting (2.25) for the corresponding part of the surface integral in (2.21). This requires the specifications of unit tangent vectors at the endpoints of the free surface. The specification of these unit vectors does not force the contact angle to have the specified value, but merely imposes a net interfacial force at the contact line. We assume that this interfacial force is given by the equilibrium surface-tension coefficients of the joining phases (Landau & Lifshitz 1958 § 145) also during flow. This level of physical modelling seems to be consistent with the assumptions inherent in (2.23) with a constant coefficient of surface tension σ.

Up to this point no specific element has been chosen. Several elements would be possible; however, we have settled on the linear quadrilateral element used also by Hassager & Bisgaard (1983) and Bach & Hassager (1984) in Lagrangian flow simulations. This means that the coordinates and the velocity field are interpolated bilinearly across each element with C^0 continuity at element boundaries, and the pressure field is constant in each element with C^{-1} continuity at element boundaries. The element is well suited for Lagrangian flow simulations since it is an isoparametric element where coordinates and velocities are interpolated with the same functions, and since the element is mass preserving as discussed by Sani *et al.* (1981), and by Crochet & Walters (1983). This means, in particular, that a fluid particle with given element coordinates remains in the same element with unchanged element coordinates

in each time step. After a certain number of time steps has been taken some elements may become excessively deformed and then a new element grid must be introduced. However, all particles are accounted for in the 'regridding' which is a straightforward procedure for Newtonian fluid simulations.

3. Formulation and numerical implementation of algorithm and a simple test problem

The method described in §2 may be formulated as an algorithm consisting of two loops: an outer time-stepping loop; and an inner coordinate iteration loop. In the inner loop the nodal velocities U_{iq} and the pressure variables P_r are calculated for any given trial configuration by solving (2.20) and (2.21) with the appropriate natural and essential boundary conditions. For this purpose, (2.15), (2.16) and the natural boundary conditions (2.25) are inserted in (2.20) and (2.21) and the algebraic equations take the form

$$A^{\nu}_{qp}\,\dot{U}^{\nu+1}_{ip}+C^{\nu}_{qir}\,P^{\nu+1}_{r}+D^{\nu}_{qpij}\,U^{\nu+1}_{pj}=F^{\nu}_{qi}+G^{\nu}_{qi}, \tag{3.1}$$

$$C^{\nu}_{qir}\,U^{\nu+1}_{iq}=0, \tag{3.2}$$

where $p,q=1,2,\ldots,N$ (number of velocity nodes); $r=1,2,\ldots,M$ (number of pressure nodes); and the spatial dimensions are $i,j=1,2$, and

$$A^{\nu}_{qp}=\rho\int_V \phi^q\phi^p\,\mathrm{d}V, \tag{3.3}$$

$$C^{\nu}_{qir}=-\int_V\left(\frac{\partial\phi^q}{\partial x_i}\right)\psi^r\,\mathrm{d}V, \tag{3.4}$$

$$D^{\nu}_{qpij}=\mu\int_V\left[\left(\frac{\partial\phi^q}{\partial x_m}\right)\left(\frac{\partial\phi^p}{\partial x_m}\right)\delta_{ij}+\left(\frac{\partial\phi^q}{\partial x_m}\right)\left(\frac{\partial\phi^p}{\partial x_i}\right)\delta_{mj}\right]\mathrm{d}V, \tag{3.5}$$

$$F^{\nu}_{qi}=-\sigma\int_{s_0}^{s_1} t_i\left(\frac{\partial\phi^q}{\partial s}\right)\mathrm{d}s-\int_{s_0}^{s_1} n_i\,P_{\mathrm{ext}}\,\phi^q\,\mathrm{d}s+\sigma[\phi^q t_i]_1-\sigma[\phi^q t_i]_0, \tag{3.6}$$

$$G^{\nu}_{qi}=\rho\int_V g_i\phi^q\,\mathrm{d}V. \tag{3.7}$$

The integrals in (3.3)–(3.7) are evaluated on configuration ν. According to (2.23), the time derivative of U_{ip} is calculated as

$$\dot{U}^{\nu}_{ip}=\frac{1}{\Delta t}(U^{\nu}_{ip}-U^{0}_{ip}). \tag{3.8}$$

The inner loop is initiated with $\nu=0$ and with estimates of nodal values of velocities and coordinates, $U^{1}_{ip}=U^{0}_{ip}$ and $x^{1}_{ip}=x^{0}_{ip}+\Delta t\,U^{1}_{ip}$, for all i and p and for some time increment Δt. Then the following three steps are performed iteratively for $\nu=1,2$ and so on:

(1) The system of linear equations in (3.2) and (3.1) with (3.8) are assembled and solved for U^{ν}_{ip} and P^{ν}_{r}.

(2) In agreement with (2.9) and (2.14) a new configuration is found from

$$x^{\nu+1}_{ip}=x^{0}_{ip}+\frac{\Delta t}{2}(U^{\nu+1}_{ip}+U^{0}_{ip}). \tag{3.9}$$

(3) The convergence of the configuration is checked by computation of δ equal to $\Sigma_{i,p}\,|x^{\nu+1}_{ip}-x^{\nu}_{ip}|/|x^{\nu+1}_{ip}-x^{0}_{ip}|$.

The iteration is continued until δ computed in step 3 is less than some prescribed value ϵ. The coefficient matrices (3.3) to (3.7) are calculated from element contributions, and these are evaluated by Gaussian quadrature with standard techniques (Cook 1974; Chung 1978).

The time-stepping loop includes the inner loop, a time increment selection procedure, and a regridding routine. The regridding routine calculates the maximum element deformation, and if it is greater than specifed, it generates a new mesh and interpolates the old solution onto the new mesh.

An accurate and easily calculated measure for element deformation is necessary if the Lagrangian method is to work effectively. We introduce the following measure:

$$D_e = \frac{V_e}{\min\limits_n J_n W_n N}, \tag{3.10}$$

where J_n is the determinant of the Jacobian matrix in the nth Gauss-point in the element e. The Gauss-weight is W_n, and N is the number of Gauss-points. The element volume (unit thickness), V_e, is:

$$V_e = \sum_n J_n W_n. \tag{3.11}$$

If an element is not deformed, D_e attains the minimum value of 1.0. As the element becomes deformed D_e increases and when the element becomes singular D_e becomes infinite. The deformation measure defined by (3.10) has several advantages over measures based on geometrical calculations, which require many expensive trigonometric calculations. The calculation of D_e is easily implemented in the element routine as the Jacobian determinants are already calculated at the Gauss-points to evaluate the Galerkin integrals (3.3) to (3.7). The deformation measure is independent of the actual element type used. This feature is especially valuable for higher-order elements. A criterion for the maximum allowable mesh deformation can be stated as

$$D_e < D_{\max} \quad \text{for all } e, \tag{3.12}$$

where $D_{\max} > 1$ is a constant.

When (3.12) is no longer fulfilled a new element mesh, which satisfies (3.12), is generated onto the old mesh. The old velocity field is then interpolated into the new mesh and the simulation may be continued.

The algorithm is implemented in an approximately 5000 statement large FORTRAN IV program. The demand for main core depends naturally on the element mesh used, and is typically in the order of 1 Mbyte in our simulations. The program is constructed to perform a regridding automatically. The need for regridding is problem dependent; in some flow situations a regridding is not even necessary and in other flow simulations we need 50 regriddings to reach a steady state. Typical CPU times are in the range 1–5 min on an IBM 3081. The program has been tested in the simulation of several standard flow situations with known analytical solutions. We present here the result of one test simulation in which a liquid rises due to capillary forces in the space between two vertical parallel plates separated by a distance a (see figure 1). To describe the position of the free surface, we introduce a rectangular coordinate system with the y-axis pointing in the vertical direction and located in the plane of symmetry, and with the x-axis pointing in the horizontal direction and located in the plane of the reference pressure. In this coordinate system the

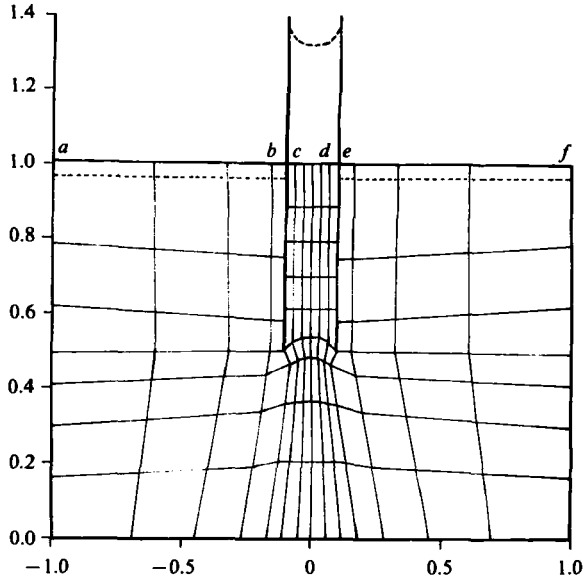

FIGURE 1. Two vertical and parallel plates are partly submerged into a fluid. The three initial free surface positions are shown with solid lines (1: *a*–*b*; 2: *c*–*d*; 3: *e*–*f*). An equilibrium contact angle of 45° is specified at *c* and *d*. The constant A (3.13) is 2.2 and the capillary length is 0.3209 cm. The equilibrium free surface position is shown as a dashed line. Length dimensions are in cm.

equilibrium position of the free surface may be expressed (Landau & Lifshitz 1959) in the parametric form:

$$x(s) = C\int_0^s \frac{\cos(s')\,\mathrm{d}s'}{[A-\cos(s')]^{\frac{1}{2}}}; \tag{3.13}$$

$$y(s) = C[A-\cos(s)]^{\frac{1}{2}}; \tag{3.14}$$

where the parameter s takes values in the interval $0 \leqslant s \leqslant T$ and $T = \pi/2-\theta$, where θ is the contact angle. In addition, C is the capillary length, $C = (2\sigma/(\rho g))^{\frac{1}{2}}$, and A is a constant determined from

$$a = C\int_0^T \frac{\cos(s')\,\mathrm{d}s'}{[A-\cos(s')]^{\frac{1}{2}}}. \tag{3.15}$$

The initial mesh used is shown on figure 1. No-slip boundary conditions are imposed on solid surfaces, except at dynamic wetting lines. Here, slip along the solid surface is imposed. Tangent vectors are specified at wetting lines: $t_a = (1,0)$, $t_b = (1,0)$, $t_c = (\alpha, -\alpha)$, $t_d = (\alpha, \alpha)$, $t_e = (1,0)$, and $t_f = (1,0)$, where $\alpha = 1/\sqrt{2}$ which implies that the equilibrium contact angle is 45° for the fluid between the plates. The final positions of the free-surface nodes between the plates are shown on figure 2 and compared to the analytical solution in (3.13)–(3.15). This example demonstrates that it is possible to include the effect of surface tension and contact angle boundary conditions with only piecewise linear, C^0 trial functions, despite the second derivative in the curvature term in the normal stress boundary condition.

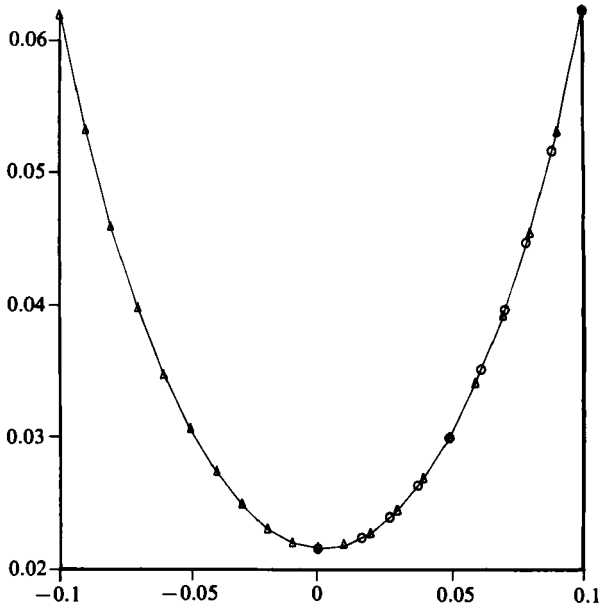

FIGURE 2. Comparison of the calculated equilibrium configuration (△); and the analytical solution (○) of Landau & Lifshitz, (3.13) and (3.14). Length dimensions are in cm.

4. Meniscus between moving parallel planes

We now present an example which is a detail of many coating processes, including both a static and a dynamic contact line. We consider a fluid between two parallel plates. The upper plate is moving with a velocity U and the lower plate is stationary. A coordinate system is oriented with the x-axis along the lower plate (see figure 3). At $x = 0$, a velocity profile satisfying the momentum equation, and the requirement of zero net flux through any plane cutting the plates, is specified,

$$u = 3U\left(\frac{y}{d}\right)^2 - 2U\left(\frac{y}{d}\right), \tag{4.1}$$

where d is the plate separation. We call this boundary the left boundary. The remaining boundary consists of the plates and a free surface. Equilibrium contact angles (equal to 45°) are specified at both contact lines through specifying the equivalent unit tangent factors. The boundary conditions specified at nodes at the wetting lines are: slip in the x-direction, and no slip in the y-direction. In this example, the capillary number $\mu U/\sigma$ is 0.033 and the Reynolds number $\rho U d/\mu$ is 2. Numerical experiments showed that the position of the left-hand boundary had no influence on the solution when it was approximately 1–2 gap widths from the free surface. The same result was found by Lowndes (1980) on a related problem.

The steady state velocity field is shown on figure 3 except for the region close to the dynamic wetting line. This region is shown on figure 4 in a considerable enlargement. The flow field near, but not at, a dynamic wetting line was given by Moffatt (1964) assuming a flat meniscus without surface tension:

$$\bar{v}_r = \frac{v_r}{U} = \frac{1}{\sin\alpha\cos\alpha - \alpha}(\cos\theta\sin\alpha - \theta\sin\theta\sin\alpha - \alpha\cos\alpha\cos\theta), \tag{4.2}$$

$$\bar{v}_\theta = \frac{v_\theta}{U} = \frac{1}{\sin\alpha\cos\alpha - \alpha}(\theta\cos\theta\sin\alpha - \alpha\cos\alpha\sin\theta). \tag{4.3}$$

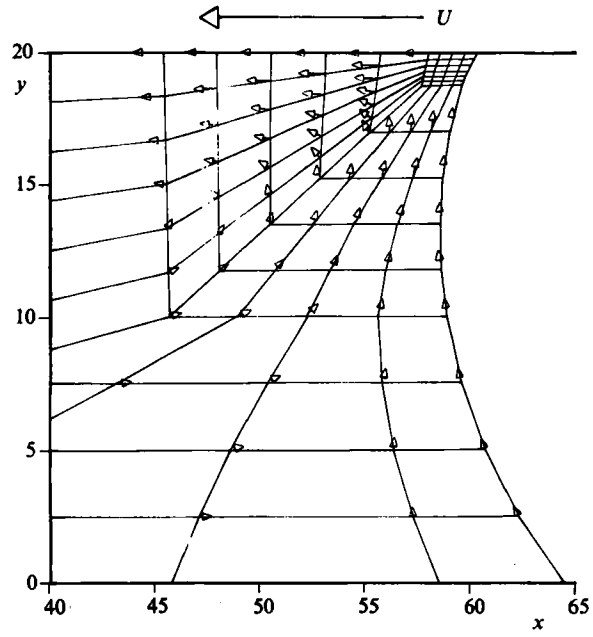

FIGURE 3. A fluid held between an upper moving plate at $y = 0.02$ cm, and a lower stationary plate at $y = 0$. The capillary number $Ca = 0.033$; and $U = 10$ cm/s. The equilibrium contact angle is 45°. At $x = 0$ a zero net flux velocity profile is specified. The steady-state velocity field is shown as velocity vectors. Note the zero normal component of the velocity vectors on the free surface. Length dimensions on x- and y-axis are 10^{-3} cm. Gravity is in the negative x-direction.

The velocity field is expressed in a plane polar coordinate system (r, θ), where r is the distance from the wetting line, and θ is the angle from the moving wall. The free surface is defined by $\theta = \alpha$. In table 1 we compare the velocity components calculated by the present algorithm at a number of points in figure 4 with those obtained from (4.2) and (4.3) in which we let $\alpha = 60°$, corresponding roughly to the location of the curved interface. We feel that the agreement is remarkably good, in view of the fact that Moffatt's solution corresponds to a completely flat interface.

In the present example the dynamic contact angle is very close to the equilibrium value. To test the situation at larger capillary and Reynolds numbers, we performed simulations with $U = 20$, 150 and 300 cm/s. The free surface for $U = 150$ and 300 cm/s, corresponding to $Re = 30$ and 60 and $Ca = 0.5$ and 1.0, is shown in figure 5. Close to the dynamic wetting line we observe the development of a 'boundary-layer' situation, wherein the meniscus slope changes rapidly to obtain a dynamic contact angle very close to the equilibrium value. We already know that viscous forces dominate inertial effects close to a wetting line. Our simulations show that (at least within the present model) capillary forces alone determine the actual dynamic contact angle and that this will equal the equilibrium contact angle for $Ca \leqslant 1$.

Since the contact angle is very difficult to measure directly at the wetting line, one usually resorts to measuring some other surface characteristic, for example, the apex height. Then, assuming a specific free-surface profile (often a part of a cylinder or sphere), it is possible to calculate an 'apparent contact angle' as the angle of intersection of the assumed profile with the wall. Our simulations show, however, that

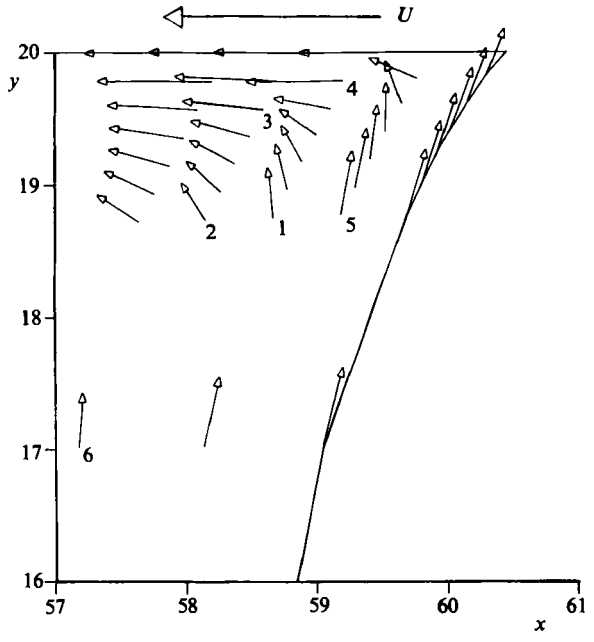

FIGURE 4. Enlargement of the dynamic wetting-line region of figure 3. The numbers refer to table 1. Length dimension is 10^{-3} cm.

		Moffatt (1964)		Present algorithm	
		$U = 10$ cm/s,	$\alpha = 70°$,	$Re = 2$,	$Ca = 0.033$,
No.	θ	$\bar{v}_r$	$\bar{v}_\theta$	$\bar{v}_r$	$\bar{v}_\theta$
1	−35	−0.11	0.26	−0.14	0.26
2	−41	0.05	0.26	0.03	0.26
3	−57	0.56	0.18	0.52	0.20
4	−60	0.66	0.15	0.65	0.12
5	−27	−0.29	0.23	−0.30	0.24
6	−28	−0.27	0.23	−0.27	0.24

TABLE 1. Comparison of normalized velocity components near a dynamic wetting line calculated by the Moffatt approximate solution and the present algorithm at different points shown in figure 4

it is not possible to fit any simple profile to the free surfaces using only one measured characteristic of the free surface, and that any such 'apparent contact angle' is not the true contact angle.

5. Advancing meniscus between fixed parallel planes

The dynamic contact line problem, formed when a meniscus moves in a capillary tube or between parallel plates, has recently been investigated theoretically by Huh & Mason (1977) and Lowndes (1980). A recent experimental investigation has been performed by Ngan & Dussan V. (1982), who made observations on the apparent contact angle dependence on the advancing speed and the gap width in a parallel-plate

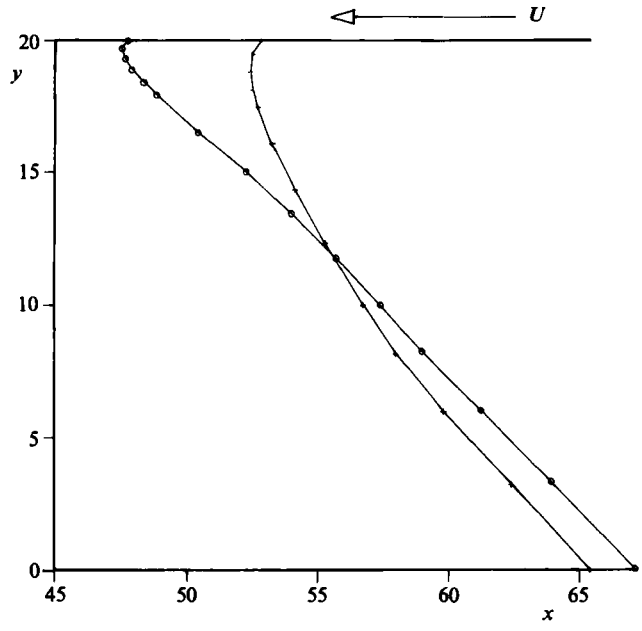

FIGURE 5. The steady-state free surface position for capillary numbers of practical interest: (+) $Ca = 0.5$, $U = 150$ cm/s; (○) $Ca = 1.0$, $U = 300$ cm/s. The geometry is the same as in figures 3 and 4. Length dimensions are in 10^{-3} cm.

geometry. Ngan & Dussan V. (1982) assume that the free surface is part of a cylinder and define the apparent contact angle θ_{app} as the intersection of this hypothetical cylinder with the plates. Then, θ_{app} may be calculated from the apex height h and the gap width $2a$ as follows:

$$\cos\theta_{app} = \frac{2(h/a)}{1+(h/a)^2}. \tag{5.1}$$

We have performed simulations in the parallel-plate geometry of Ngan & Dussan V. Due to the symmetry only one of the symmetric parts needs to be included in the simulation. The wetting-line boundary conditions are identical to the previous example. Zero shear stress and zero normal velocity are specified at the symmetry plane. At the intersection line between the free surface and the symmetry plane a unit tangent vector $t_0 = (0, 1)$ is specified. A parabolic inflow velocity profile is specified at $x = 0$.

On figure 6 the steady-state velocity field is shown in a coordinate system moving with the wetting-line velocity U. In table 2 the calculated solution is compared with Moffatt's local solution. The agreement is very good, which implies as expected that the viscous terms alone determine the velocity field near the wetting line. The surface tension seems to affect only the pressure field and the free-surface shape.

Ngan & Dussan V. (1982) have reported values of the apparent contact angle measured in a parallel plate geometry for three different gap widths. Their main conclusion is that θ_{app} not only depends on the capillary number Ca, but also on a. To test the influence of a, we performed two simulations with $a = 0.005$ cm and $a = 0.035$ cm, respectively, and with $Ca = 0.02$ in both simulations. In all simulations we prescribe an equilibrium contact angle equal to 35°. We arrived at this particular value by extrapolation to zero capillary number in table 4, p. 33 of Ngan & Dussan

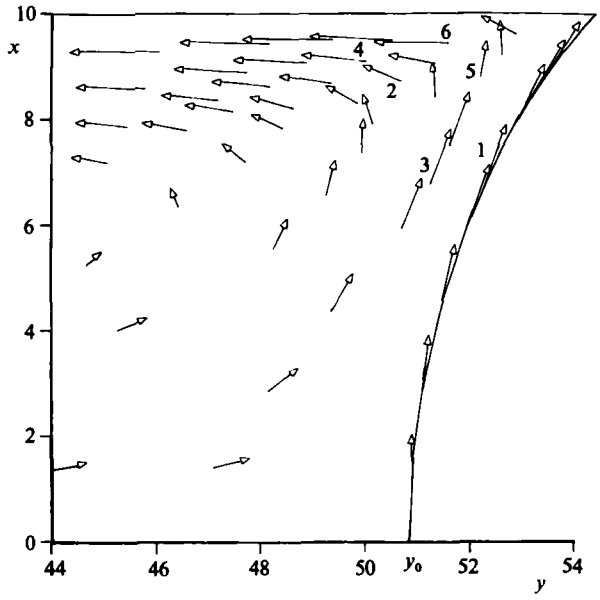

FIGURE 6. The symmetry part of a fluid advancing between two parallel plates. At $y = 0$ a semiparabolic velocity profile is specified. The velocity vectors are shown in a coordinate system moving with the contact line velocity. The numbers refer to table 2. The capillary number is $Ca = 0.01$, and length dimensions are in 10^{-3} cm. Gravity is in the negative y-direction.

		Moffatt (1964)		Present algorithm	
		$U = 0.0203$ cm/s,	$\alpha = 60°$,	$Re = 2 \times 10^{-4}$,	$Ca = 0.01$
No.	θ	$\bar{v}_r$	$\bar{v}_\theta$	$\bar{v}_r$	$\bar{v}_\theta$
1	0	−0.54	0	−0.51	0
2	−41	0.24	0.20	0.23	0.20
3	−15	−0.44	0.14	−0.43	0.14
4	−48	0.51	0.16	0.53	0.16
5	−32	−0.07	0.22	−0.09	0.21
6	−50	0.59	0.14	0.59	0.11

TABLE 2. Comparison of normalized velocity components near a dynamic wetting line calculated by the Moffatt approximate solution and the present algorithm at different points shown on figure 6. Note: the wetting-line velocity U has been subtracted from the velocity field calculated by the present algorithm.

V. (1982). The results are summarized in table 3 and figure 7. The agreement between the calculated and measured apparent contact angles is remarkably good. Calculations 2 and 3 (table 3) show that the assumptions of negligible inertial and gravity influence, made by Ngan & Dussan V. (1982), are correct. Neither the Reynolds number ($Re = \rho U a/\mu$) nor the Bond number ($Bd = \rho g a^2/\sigma$) has any influence on θ_{app}. As the capillary number is the same in the two simulations, and as Re and Bd have no influence, the same solution should be found if no other parameters entered the problem. The experiments of Ngan & Dussan V. (1982) show that one does not find the same h/a values, which implies that one more parameter must enter in a model of flows containing dynamic contact lines. The agreement between the experiments

	a (cm)	$Re \times 10^5$	$Bd \times 10^3$	$Bs \times 10^3$	Calculated $\cos\theta_{app}$	Calculated θ_{app}	Measured θ_{app}
1	0.005	2.0	1.2	56.0	0.588	54.0	54 ± 1.5
2	0.035	14.0	59.0	8.0	0.453	63.1	63 ± 1.5
3	0.035	14.0	1.2	8.0	0.453	63.1	
4	0.035	2.0	59.0	8.0	0.455	63.1	

TABLE 3. Comparison of calculated and measured (Ngan & Dussan V. 1982) values of the apparent contact angle for two different gap widths. The capillary number is constant $Ca = 0.02$. The slip number is defined as $Bs = \tau U/a$ where τ is the reorientation time. Equilibrium contact angle = 35° in all simulations

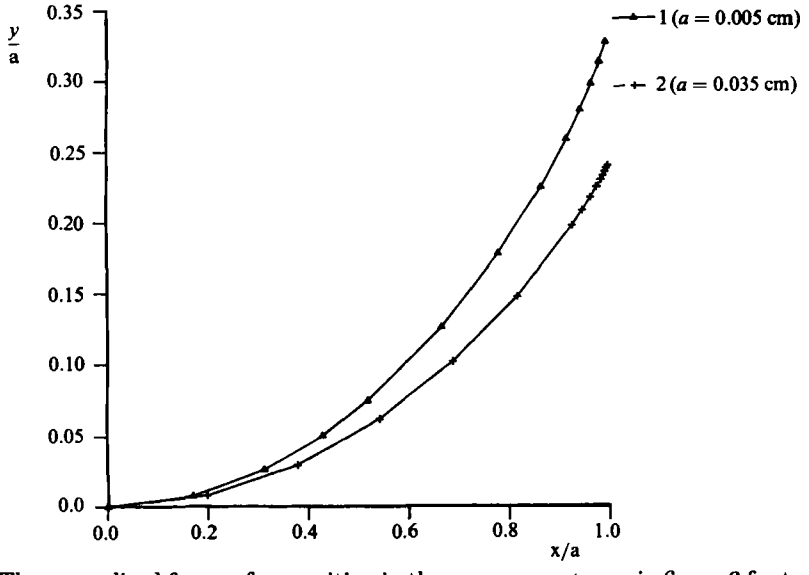

FIGURE 7. The normalized free surface position in the same geometry as in figure 6 for two different plate distances, with constant capillary number $Ca = 0.02$. The y coordinate is $y - y_0$, where y_0 is the intersection point between the symmetry plane and the free surface. The apparent contact angles are listed in table 3.

and the simulations shows that Navier–Stokes equations with the presented slip boundary conditions can be used as a valid model for such flows. The additional parameter enters through the boundary conditions at the wetting line. Here the fluid is allowed to slip over some distance β. The physical interpretation of this model is that the molecules need a finite 'slip time', τ, to complete their bonds to the solid interface. During the time τ the wetting line moves the distance $\beta = \tau U$. Unfortunately, there seems to be no theory nor measurements from which τ can be found directly. The slip time can also be considered just as a model parameter, which has to be estimated in the model from some suitable experiments. The results in table 3 have been obtained with $\tau = 7 \times 10^{-4}$ s in all simulations. If more data were present, it would be possible to test whether the slip time is a unique physical property of the fluid and the solid.

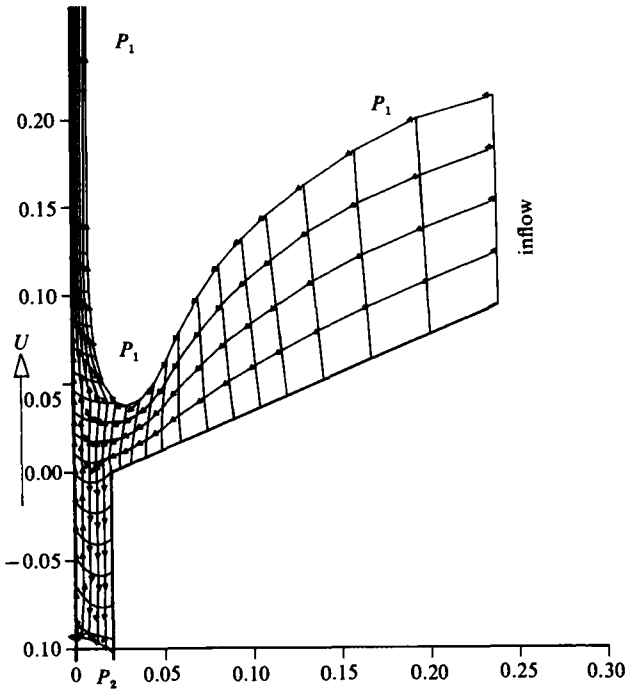

FIGURE 8. Slide coating. The capillary number is $Ca = 0.58$; the Reynolds number is $Re = 33.3$. The Bond number is $Bd = 0.02$. The dimensionless inflow rate is $\bar{q} = 0.5$, and the dimensionless pressure difference is -30. Length dimensions are in cm.

6. Slide coating

Kistler & Scriven (1983) have very recently reviewed computational methods for coating flows. To illustrate the capability of the implementation of our algorithm, we have chosen one of their industrial coating flows, the slide-coating flow, shown on their figure 8.7*g*. In this coating process there are two free surfaces and two contact lines at the lower free surface. To obtain the steady state shown on figure 8, a pressure difference ($P_1 - P_2 < 0$) must be specified. In the situation shown, the ultimate film thickness is reached very fast. With other parameters the film-forming zone may extend far downstream. Since it is advantageous to perform the slide-coating operation as fast as possible, it is important to find conditions under which the flow is stable. Indeed the steady state shown in figure 8 is reached in a two-dimensional transient calculation, we conclude that will not be unstable to a two-dimensional disturbance. The same conclusion cannot be reached on the basis of the Eulerian steady-state simulation cited by Kistler & Scriven without a separate stability analysis, and this then illustrates an advantage of the Lagrangian approach.

7. Discussion

It has been demonstrated that the proposed algorithm for the use of the Lagrangian kinematic specification may be implemented with the aid of the finite-element method. The method has been shown to have considerable flexibility with a wide range of boundary conditions.

The algorithm consists of an outer time-stepping loop and an inner coordinate

iteration loop. By reducing the time step in the outer loop, the desired velocity in the inner loop can be made arbitrarily close to the known velocity in the previous time step. No formal proof of convergence is given but in all examples shown here the convergence in the velocity iteration loop is better than linear.

In order to obtain convergence of finite-difference solutions at high Reynolds numbers it is customary (Roache 1976) to use 'upwinding' techniques. Roughly speaking the need for upwinding arises when the convective terms dominate the viscous terms. In the present technique no such additional devices are needed or even possible since 'upwinding' is in a natural way included with use of a Lagrangian specification.

Moving contact lines are modelled with minute slip at the contact line and contact angles are included as natural boundary conditions. The agreement between the theoretical predictions and the experimental results of Ngan & Dussan V. in §5 provides evidence that this is a valid model. It has also been demonstrated that, within this model, the true contact angle will remain equal (or nearly equal) to the equilibrium contact angle at least up to capillary numbers $O(1)$. Consequently, our model is in agreement with that of Hocking (1981) and Lowndes (1980) who impose the contact angle as an essential boundary condition. The model is, however, different from that of Kistler & Scriven (1983) who introduce a 'dynamic contact angle' which is different from the equilibrium contact angle. Our simulations do not support this notion, but more experimental evidence may be needed to decide between the models.

We demonstrate how the theoretical predictions may be used to obtain information about the slip time from experimental measurements, and the need for such measurements is reiterated.

We wish to acknowledge financial assistance provided by the Danish Council for Scientific and Industrial Research. We thank the Department of Chemical Engineering and the Mathematics Research Center of the University of Wisconsin, Madison, for hospitality during manuscript preparation. We would like to thank Professor E. B. Dussan V. for helpful correspondence.

REFERENCES

BACH, P. & HASSAGER, O. 1984 A Lagrangian finite element method for the simulation of flow of Newtonian liquids. *AIChE J.* **30**, 508.

BACH, P. & VILLADSEN, J. 1984 Simulation of the vertical flow of a thin wavy film using a finite element method. *Intl J. Heat and Mass Transfer* **27**, 815.

BIRD, R. B., ARMSTRONG, R. C. & HASSAGER, O. 1977 *Dynamics of Polymeric Liquids, Vol. I; Fluid Dynamics.* Wiley.

CHUNG, T. J. 1978 *Finite Element Analysis in Fluid Dynamics.* McGraw-Hill.

COOK, R. D. 1974 *Concepts and Applications of Finite Element Analysis.* Wiley.

CROCHET, M. J. & WALTERS, K. 1983 *Computational Techniques for Visco-elastic Fluid Flow.* In *Computational Analysis of Polymer Processing* (eds. J. R. A. Pearson & S. M. Richardson). New York: Applied Science Publishers.

HASSAGER, O. & BISGAARD, C. 1983 A Lagrangian finite element method for the simulation of flow of non-Newtonian liquids. *J. Non-Newtonian Fluid Mech.* **12**, 153.

HIRT, C. W., COOK, J. L. & BUTLER, T. D. 1970 A Lagrangian method for calculation of the dynamics of an incompressible fluid with free surface. *J. Comp. Phys.* **5**, 103.

HOCKING, L. M. 1981 Sliding and spreading of thin two-dimensional drops. *Q. J. Mech. Appl. Maths* **34**, 37.

HUH, C. & MASON, S. G. 1977 The steady movement of a liquid meniscus in a capillary tube. *J. Fluid Mech.* **81**, 401.

KISTLER, S. F. & SCRIVEN, L. E. 1983 Coating flows. In *Computational Analysis of Polymer Processing* (eds J. R. A. Pearson & S. M. Richardson). New York: Applied Science Publishers.

LANDAU, L. D. & LIFSHITZ, E. M. 1958 *Statistical Physics*. Pergamon.

LANDAU, L. D. & LIFSHITZ, E. M. 1959 *Fluid Mechanics*. Pergamon.

LOWNDES, J. 1980 The numerical simulation of the steady movement of a fluid meniscus in a capillary tube. *J. Fluid Mech.* **101**, 631.

MOFFATT, H. K. 1964 Viscous and resistive eddies near a sharp corner. *J. Fluid Mech.* **18**, 1.

NGAN, C. G. & DUSSAN V., E. B. 1982 On the nature of the dynamic contact angle: an experimental study. *J. Fluid Mech.* **118**, 27.

ROACH, P. J. 1976 *Computational Fluid Dynamics*. Albuquerque: Hermosa Publishers.

RUSCHAK, K. J. 1980 A method for incorporating free boundaries with surface tension in finite element fluid-flow simulators. *Intl J. Numer. Meth. Engng* **15**, 639.

SANI, R. L., GRESHO, P. M., LEE, R. L. & GRIFFITHS, D. F. 1981 The cause and cure (?) of the spurious pressure generated by certain FEM solutions of the incompressible Navier–Stokes equations: Part 1. *Intl J. Numer. Meth. Fluids* **1**, 17.

SOKOLNIKOFF, I. S. & REDHEFFER, R. M. 1966 *Mathematics of Physics and Modern Engineering*. McGraw-Hill.

TANNER, R. I. 1983 Extrudate swell. In *Computational Analysis of Polymer Processing* (eds J. R. A. Pearson & S. M. Richardson). New York: Applied Science Publishers.